SEMARAK ILMU PUBLISHING

CFD Letters

Journal homepage:
https://semarakilmu.com.my/journals/index.php/CFD_Letters/index
ISSN: 2180-1363

Concentrated Flow Effects on Aerodynamics Performance for CyFlaP Magnus UAV by using Computational Approach

Hidayatullah Mohammad Ali[1,*], Azmin Shakrine Mohd Rafie[1], Mohd Faisal Abdul Hamid[1], Syaril Azrad Md Ali[1]

[1] Department of Aerospace Engineering, Faculty of Engineering, Universiti Putra Malaysia, 43400 Serdang, Selangor, Malaysia

ARTICLE INFO

Article history:
Received 12 April 2025
Received in revised form 14 May 2025
Accepted 14 June 2025
Available online 17 July 2025

Keywords:
Aerodynamic coefficients; concentrated flow; flat plate; Magnus UAV; rotating cylinder

ABSTRACT

The Cylinder-to-Flat Plate embedment (CyFlaP) Magnus Unmanned Aerial Vehicle (UAV) utilises a rotating cylinder propulsion mechanism that benefits from the Magnus effect to enhance aerodynamic performance. While previous studies have demonstrated that this design generates substantial lift, the presence of large flow separation bubbles atop the surface remains a critical limitation, leading to increased drag and reduced aerodynamic efficiency. To address this issue, this study investigates the effects of concentrated airflow on the aerodynamic characteristics of the CyFlaP by incorporating a fixed top plate above the model. By directing airflow over the rotating cylinders, the top plate is hypothesised to mitigate separation effects and enhance lift. This approach optimises the Magnus effect while reducing aerodynamic inefficiencies caused by flow separation bubbles. A computational fluid dynamics (CFD) analysis was conducted using ANSYS Workbench to evaluate aerodynamic performance under varying conditions. The study parameters included inlet wind speeds ranging from 5 m/s to 15 m/s, gap sizes between the top plate and the main structure varying from 5 mm to 30 mm and angles of attack from 0° to 20°. The k-omega Shear Stress Transport ($k-\omega$ SST) turbulence model was employed to capture flow separation and vortex formation accurately. The results indicate a significant enhancement in lift coefficient (C_L), with improvements of up to 120% compared to reference values. The study also reveals that smaller gap configurations between the top plate and the CyFlaP structure facilitate better concentrated airflow, effectively reducing separation bubbles and improving overall aerodynamic efficiency. Additionally, the modified design demonstrated a delay in stall onset at higher angles of attack, which is crucial for maintaining lift at increased wind speeds. However, the findings also suggest that while lift is improved, drag values increase at higher speeds, indicating the need for further design refinements, such as smoothing the leading edge of the top plate. In conclusion, the incorporation of a top plate in the CyFlaP Magnus UAV significantly enhances aerodynamic performance by optimising concentrated airflow. These findings establish a foundation for optimising top plate configurations in Magnus UAVs, offering a potential path to enhanced lift efficiency and reduced aerodynamic losses.

* *Corresponding author.*
E-mail address: hidayatullah@upm.edu.my (Hidayatullah Mohammad Ali)

https://doi.org/10.37934/cfdl.18.3.134151

1. Introduction

Aerodynamics is the way how an object moves through the air. Anything that moves through the air is generally affected by aerodynamics, from a flying kite to a rocket blasting off into the sky. At low speed, per se, the surface body is aerodynamically in shape; the airflow may split when encountered by an object and then flow surrounding its surface body. However, faster wind speed may result in airflow tending to break away and become turbulent. Nonetheless, the turbulence may form a separation flow on top of the object, which further worsens at a higher angle of attack (α) and sooner eventuate a stall.

In 2021, Ali *et al.*, [1] reported that the Cylinder-to-Flat Plate embedment (CyFlaP) enhanced aerodynamic performances, achieving up to a 76% increase in the coefficient of lift (C_L) and a 99% reduction in the coefficient of drag (C_D), respectively. Here, the CyFlaP Magnus Unmanned Aerial Vehicle (UAV) embodiment consisted of a dual rotating cylinder, each incorporated on a flat plate leading and trailing edge. The rotating cylinder acts as the propulsion mechanism for the model, benefiting from the Magnus effects, which generate lift when acted upon the incoming air.

The study of the Magnus effects on a bluff body has been done for almost a century to date yet the improved C_L and C_D have not been able to entirely reduce the formation of separation flow on the surface body. Ali *et al.*, [2] depicted that the formation of high flow separation may cause larger swirling vortices at a high angle of attack. The implementation of the rotating cylinder helped in ensuring stall angle delay at a high angle of attack. Still, additional support would be needed to reduce the arising matter even further, which may be noted in its coefficient's improvement.

Meanwhile, Modi [3] has numerically proved that the double cylinder embedment may only generate a high lift for a specific range of angle of attack depending on the placement of the cylinder. Moreover, another double cylinder investigation by Modi *et al.*, [4] has resulted in a lower C_D at a higher velocity ratio (V_r). Nil mentioned its C_L but this results best noted the capability of the rotating cylinder on reducing its C_D hence, the separation bubble can be reduced here within. Furthermore, a study on the double-rotating cylinder by Guo *et al.*, [5] has performed well in a side-by-side arrangement at an increasing rotational speed pace. Still, the matter can only be achieved with a constant concentrated airflow onto the model's bluff body. Following that, Alias *et al.*, [6] has proven the ability of their device incorporating rotating cylinder to generate lift for a very short take-off about the right concentrated airflow setup.

Recent investigations by Ali *et al.*, [7] further supported this by showing that double rotating cylinders on the Selig S1223 aerofoil and flat plate could enhance lift and delay stall due to the Magnus effect, indicating the potential for improved aerodynamic efficiency in high-altitude platforms. However, Arif *et al*., [8] found that although ducted fans increased lift on flat plates, they did not fully counteract destabilising pitching moments, emphasising the need for additional design modifications. In exploring drag reduction, Kamid *et al.*, [9] demonstrated that higher rotational speeds of cylinders effectively minimised flow separation around bluff bodies. Additionally, Roslan *et al.*, [10] highlighted that increased rotational speeds of double cylinders not only enhanced lift but also reduced drag on flat plates, showcasing their potential for improved aerodynamic performance. Furthermore, Zaimi *et al*., [11] experimentally confirmed that strategic placement and speed adjustment of embedded rotating cylinders could effectively influence pitching moments, providing valuable insights for enhancing stability in high-altitude platforms by manipulating flow structures, including separation bubbles, which in turn suppress separation bubble formation and improve the performance, aerodynamically.

Magnus-based UAV designs that utilise rotating cylinders. Have demonstrated significant aerodynamic advantages, particularly in lift generation and stall delay. However, optimising airflow

behaviour remains a key area of research that is needed to enhance aerodynamic efficiency further. Studies by Ali *et al.,* [1,2] have shown that the CyFlaP Magnus UAV, which incorporates rotating cylinders, achieves improved lift characteristics. While these studies provide valuable insights, there is still potential to refine flow control strategies to enhance aerodynamic performance. Research by Modi [3] and Guo *et al.,* [5] has further explored double-cylinder configurations, demonstrating their effectiveness in generating lift. However, the influence of additional external structures in shaping and directing airflow for more consistent aerodynamic benefits remains an area requiring further investigation.

Most existing approaches rely on cylinder rotation to modify airflow, which contributes to lift enhancement. However, there is a limited investigation into how an external structure, such as a top plate, can actively direct and concentrate airflow over the body to improve aerodynamic performance. The presence of a top plate above the CyFlap structure is expected to regulate the airflow, minimising excessive separation while enhancing lift and delaying stall. This concept introduces an alternative method for improving the efficiency of Magnus-based UAV designs.

The present study proposes a modified CyFlaP configuration incorporating a fixed top plate to explore this approach. A computational fluid dynamics (CFD) analysis is conducted to evaluate the effects of different top plate gap sizes on aerodynamic characteristics, particularly in terms of lift and drag performance. This study aims to provide a better understanding of airflow control mechanism in Magnus UAV applications, offering insights for optimising aerodynamic performance and guiding future design improvements in aerial vehicles.

2. Methodology

2.1 Geometry Configurations

This study employs CFD to analyse the aerodynamic performance of the CyFlaP Magnus UAV. The computational process follows a structured workflow, beginning with geometry configuration, followed by the selection of an appropriate turbulence model, defining key performance parameters, generating a computational grid, setting up the solver and finally, performing validation to ensure accuracy. A similar computational flow has been effectively applied in UAV aerodynamic studies, as highlighted by Subramaniam *et al.*, [12], demonstrating the importance of a systematic approach in CFD modelling.

The design parameters for this research project are implemented using the CyFlaP as the base design for this study. The CyFlaP is adopted per the study by Ali *et al.*, [1] where the model consists of a double rotating cylinder embedded in the front and the back end of a flat plate. Therefore, the parameters set in this research study were set based on the available resources data from the preferred embodiment of choice, Wang *et al.*, [13].

The CyFlaP is designed to generate high lift while delaying stall onset at higher angles of attack. This configuration would not be achievable without the in-depth selection of proper individual specifications for testing, i.e. the cylinder dimension, size, flat plate length, etc. The most crucial aspect to consider when deciding on the design is the Magnus capability of the rotating cylinder itself. Badalamenti *et al.,* [14] showed tremendous results when comparing the rotating cylinder with other end configurations from his past research works. The cylinder configuration was hereby taken from his mere work with an aspect ratio (AR) of 5.1 calculated with the following Eq. (1):

$$\mathrm{AR} = \frac{\mathrm{s}^2}{\mathrm{A}} = \frac{\mathrm{s}^2}{\mathrm{sc}} = \frac{\mathrm{s}}{\mathrm{c}} \tag{1}$$

where s is the span of the cylinder, A is the area and c are the cylindrical chord.

As for the CyFlaP, the diameter is converted at a diameter (D) of 160 mm. The rotating cylinder is set clockwise to simulate the same condition run by Badalamenti *et al.,* [14] and Ali *et al.*, [1,2]. This clockwise direction setting was propounded from the study by Barati *et al.*, [15]. This will ensue in an up-force lift generation when the induced flow flows atop the model while having vice versa action on the bottom part of the cylinder.

Next, Ali *et al.,* [1,2] adopted his flat plate design from Wang *et al.*, [13] and Torres [16] where they denoted a maximum lift coefficient (C_{Lmax}) achieved at approximately 60% for their highest angle of attack. The design is preset with a flat plate length of 1.00 m. The term CyFlaP was introduced by Ali *et al.*, [1]. Still, the embodiment investigation of double rotating has been available for more than three decades ago and previously was focused on computational testing on an aerofoil by Modi [3] and Modi *et al.*, [4]. A top plate fixture was added to the CyFlaP to create a concentrated flow over the design. Refer to Figure 1, where 1(a) shows the original design from Ali *et al.,* [1,2] and 1(b) illustrates the modified version with the attached top plate.

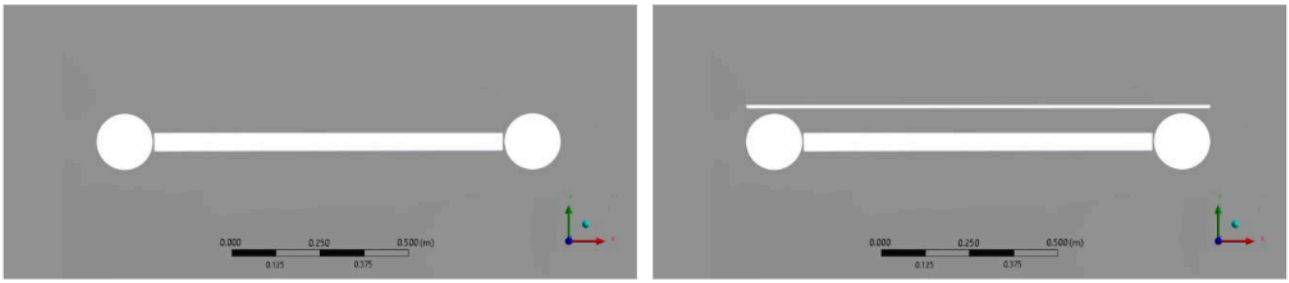

(a) (b)

Fig. 1. Geometry of CyFlaP with (a) Original reference geometry from Ali *et al.,* [1,2] (b) Modified version with top flap

The gap on the embedment was set at 5 mm apart from the cylinders-flat plate-top plate configurations to represent an optimum performance with reference from the study by Abdulla *et al.,* [17], together with a length from end-to-end, plus a thickness of 5 mm.

2.2 Turbulence Model

The turbulence modelling in this research denoted the use of mathematical models to solve the intended configuration, hence forecasting the impact of turbulence on its surface body. Currently, the shear stress transport (SST) K-ω model is suited well for the research work with reference from Ali *et al.*, [1,2] and Mgaidi *et al.*, [18] which incorporated extra transport equation denoted as K for the first transported variable, while the second transported variable as ω for its specific dissipation on solving the matter.

The SST K- ω model by Menter [19] was duly selected to employ the K- ω model in the near-wall region with the one away from the model in the far field. Concurrently, the amalgamation resulting from the SST was merely a formation from the combination of K-ω and K-ε, respectively. This will reduce the error that arises in the inlet of the free-stream turbulence properties. In the ANSYS Fluent, the general form of the SST K- ω transport equation is dented as per the following:

$$\frac{\partial}{\partial t}(\rho k) + \frac{\partial}{\partial x_i}(\rho k u_i) = \frac{\partial}{\partial x_j}\left[\Gamma_k \frac{\partial k}{\partial x_j}\right] + G_k - Y_k + S_k \tag{2}$$

$$\frac{\partial}{\partial t}(\rho \omega) + \frac{\partial}{\partial x_i}(\rho \omega u_i) = \frac{\partial}{\partial x_j}\left[\Gamma_\omega \frac{\partial \omega}{\partial x_j}\right] + G_\omega - Y_\omega + S_\omega \tag{3}$$

Eq. (2) and Eq. (3) generally relate the turbulence kinetic energy to the mean velocity gradient and the production of ω, presented as G_k and G_ω, respectively. Concurrently, Γ_k and Γ_ω represent the effective diffusivities of k and ω due to turbulence. Next, the Y_k and Y_ω represented the dissipation of k and ω and lastly, the S_k and S_ω denoted on the user-defined source terms.

2.3 Key Performance Parameter

The key performance parameter (KPP) hereby generically signifies the performance goal in this study. The aerodynamic performance from the post-processing results is evaluated using the C_L and C_D formulas shown in Eq. (4) and Eq. (5), respectively.

$$C_L = \frac{L}{\frac{1}{2}\rho V^2 S} \tag{4}$$

$$C_D = \frac{D}{\frac{1}{2}\rho V^2 S} \tag{5}$$

where L is the lift force while D is the drag force of the model, ρ is the density of the fluid, i.e. air, V is the inlet velocity and S is the area of the projected model. Duly noted that both the C_L and C_D are curated as dimensionless normalisation of the amount of lift or drag produced by the model.

2.4 Grid Generation

The pre-processing measures for this research require a mesh suitable for the boundaries and appropriate meshes for the two-dimensional (2D) computational runs. The specifications are described here, along with its domain and boundaries, which are known as the grid generation. Here, the most crucial step in CFD is to get the right part for the CFD analysis where a quality grid generated would reflect result-wise.

The meshes are formed based on the study by Ali *et al.*, [1,2] and Yao *et al.*, [20] where he incorporated double rectangular blocks to set a few meshes type, i.e. quadrilateral and triangular elements. In this setup, D represents the diameter of the rotating cylinder, which serves as a reference length for defining the computational domain. Here, the inner zone with a dimension of 2D x 3D block and an outer zone of 6D x 15D is set up accordingly, refer to Figure 2(a). Additionally, atop the model's surface body, the surfaces were fixed with y-plus (y+) of less than 1 together with an inflation criterion of 10 layers at a growth rate of 1.2 setups from the wall to its first mesh nodes, refer to Figure 2(b) and 2(c). This will ensure that the wall function approach is to be attained confidently for this turbulence condition and/or model.

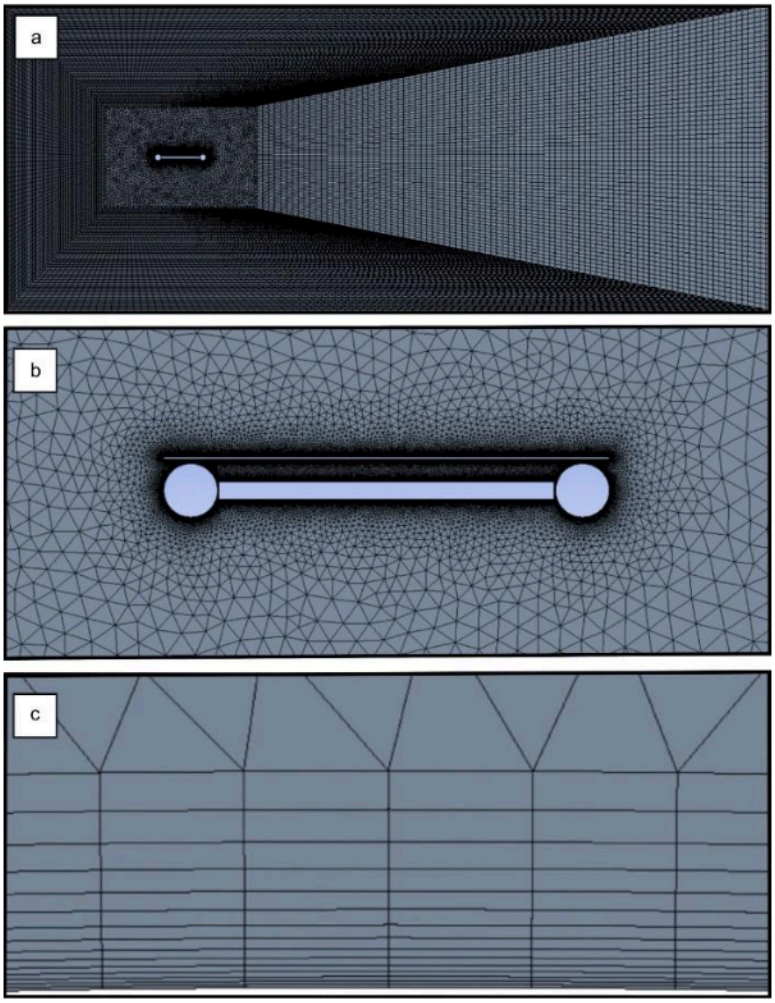

Fig. 2. CyFlaP's domain and meshes (a) from domain configuration (b) mesh near the model (c) to the inflation on the surface body

The boundary conditions and mesh setup were carefully configured to ensure accurate aerodynamic analysis, as detailed in Table 1 and Table 2. These configurations were selected based on insights from previous research to optimise data accuracy and reliability. The velocity-inlet boundary condition is applied at the inlet to define the incoming airflow speed, ensuring realistic flow behaviour. In contrast, a pressure-outlet condition at the exit allows airflow to leave the domain smoothly without reflection. The leading and trailing edge cylinders, along with the flat plate and top plate, are defined as walls to impose no-slip conditions, accurately capturing boundary layer effects essential for analysing the Magnus effect. A symmetry condition is applied at the top boundary to simulate an infinite flow domain, preventing artificial disturbances. At the same time, interior surfaces are designated as 'Interior' to facilitate proper flow communication between different mesh regions.

Table 1
Boundary conditions

Boundary conditions	Type
Inlet	Velocity-inlet
Outlet	Pressure-outlet
Cylinder – leading edge	Wall
Cylinder – Trailing edge	Wall
Flat plate	Wall
Top plate	Wall
Wall	Symmetry
Interior surface body	Interior
Surface body	Interior

The mesh setup is designed for optimal resolution and computational efficiency, as shown in Table 2. A growth rate of 1.2 is used to gradually increase the mesh size away from the walls, ensuring high detail near the surface where flow gradients are steep. The defeature size is set to 3.5×10^{-4} m and the curvature minimum size is 7.0×10^{-4} m, providing an accurate representation of geometric features. A curvature normal angle of $18°$ is used to maintain mesh quality around curved surfaces, while high smoothing is applied to optimise element transitions. Inflation layers are implemented to resolve the boundary layer with a first layer thickness option, 10 maximum layers and a growth rate of 1.2, enhancing the accuracy of wall function approaches under turbulent flow conditions. This comprehensive boundary condition and mesh setup strategy are crucial for achieving reliable and precise aerodynamic performance predictions.

Table2
Mesh setups

Mesh specifications	
Growth rate	1.2
Defeature size	3.5e-004 m
Curvature minimum size	7.0e-004 m
Curvature normal angle	18.0°
Smoothing	High
Inflation specifications	
Inflation option	First layer thickness
Maximum layers	10
Growth rate	1.2

Therefore, before commencing further into the solver setting, a mesh independency test (MIT) would be best to apprehend the data viable for this research study. Here, the MIT for the CyFlaP from Ali *et al.,* [1] has been tested to test the mesh stability in providing the best data quality to the available resources. In this case, the grid refinement of 1.64E+05 yielded less than 1% error, hence reliably best used for the CFD testing, refer to Figure 3.

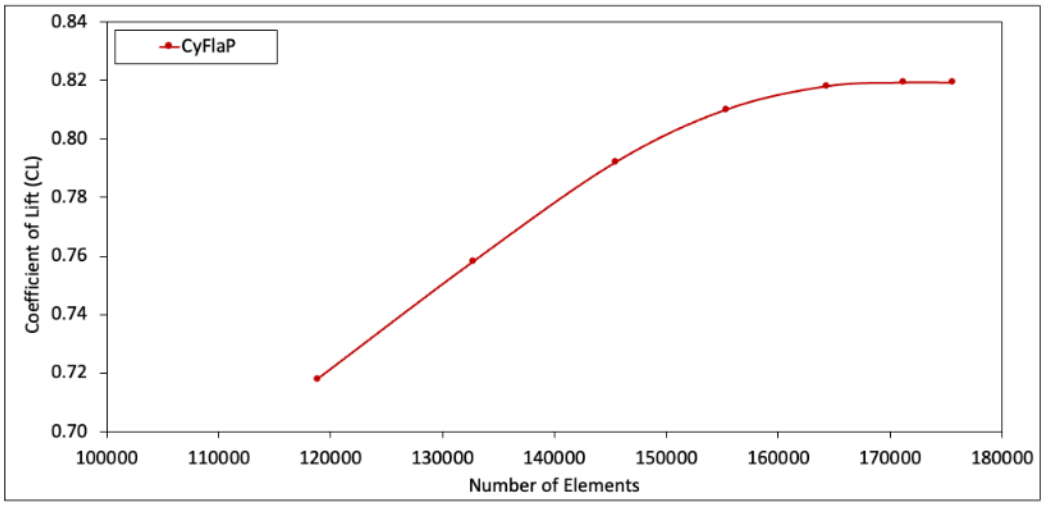

Fig. 3. CyFlaP's MIT test results

2.5 Solver Setting

From the turbulence model to reference values, then to spatial discretisation, the solver setting is utterly the utmost step in the CFD solver interface before commencing further into the solution calculations. These inputs introduce the concepts of accuracy, stability and convergence that each can understand. Here, the best setup has been listed as per the following to scrutinise the numerical simulations best, refer to Table 3.

Table 3
Solver settings

General	
Type	Pressure-based
Velocity formulation	Absolute
Time	Transient
2D space	Planar
Model	
Viscous	SST k-omega
Reference values	
Density (kg/m3)	1.225
Pressure (pascal)	101325
Temperature (K)	288.16
Velocity (m/s)	5,10,15
Viscosity (kg/m-s)	1.789e-005
Solution	
Method	Pressure-velocity coupling
Scheme	Coupled
Residual error	1.e-006
Spatial discretization	
Gradient	Green Gauss Node Based
Pressure	PRESTO!
Momentum	QUICK
Turbulent kinetic energy	QUICK
Specific dissipation rate	QUICK

2.6 Validation

Before processing deeper into the simulation testing, a validation study should be done before conforming to the evidence to support the effectiveness of using the flat plate as a top plate compared to the available data resources. Here, data resources by Badalamenti *et al.,* [14] and Torres [16] were used to cater to the need to validate their data with the one tested computationally.

Figure 4 depicts satisfactory results with the available resources, strengthening the idea of using it for this research's main top plate design. These findings provide a strong basis for further simulations, ensuring the flat plate's design reliability and demonstrating consistency between computational and experimental data.

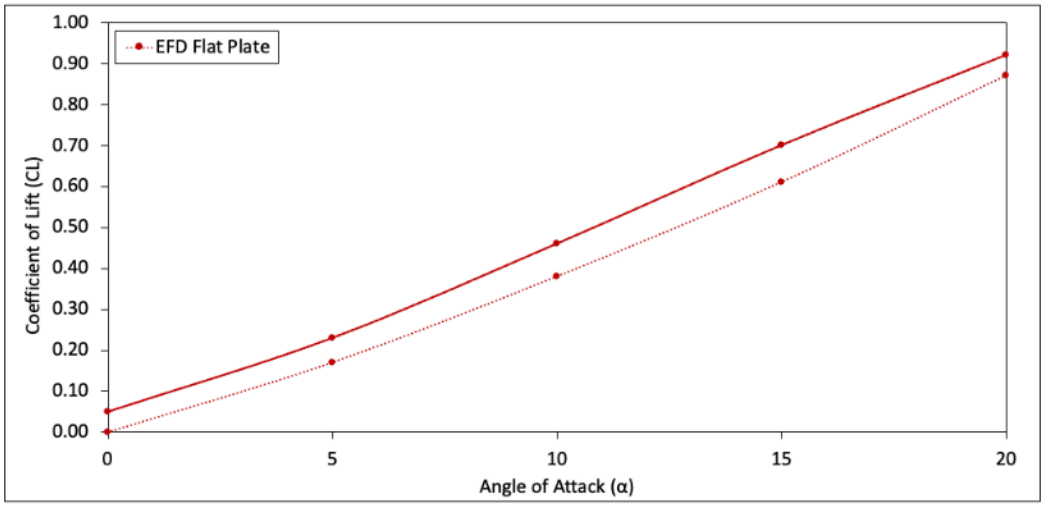

Fig. 4. Validation of flat plate for top plate application

3. Results

3.1 Effect of Geometric and Flow Parameters on Force Coefficients

The post-processor results are hereby computed based on their parameters:

i. with gap difference from a top plate atop of the model ranging from 5 mm to 30 mm at an interval of 5 mm
ii. with an inlet speed of 5, 10 and 15 m/s
iii. at 5 degrees (°) interval of α from 0° to 20°.

The gap of 5 mm was fixed for CyFlaP embedment between the cylinder and the flat plate at all conditions. Moreover, the rotational speed of the cylinder was set to fix at 1000 revolutions per minute (RPM) for this study before mimicking the rotation tested by Ali *et al.*, [1,2]. Figure 5 to Figure 7 depict the data results, which establish a relationship between the output from the ANSYS results in terms of C_L, C_D and α. A reference line was set for reference guidance on comparing the data.

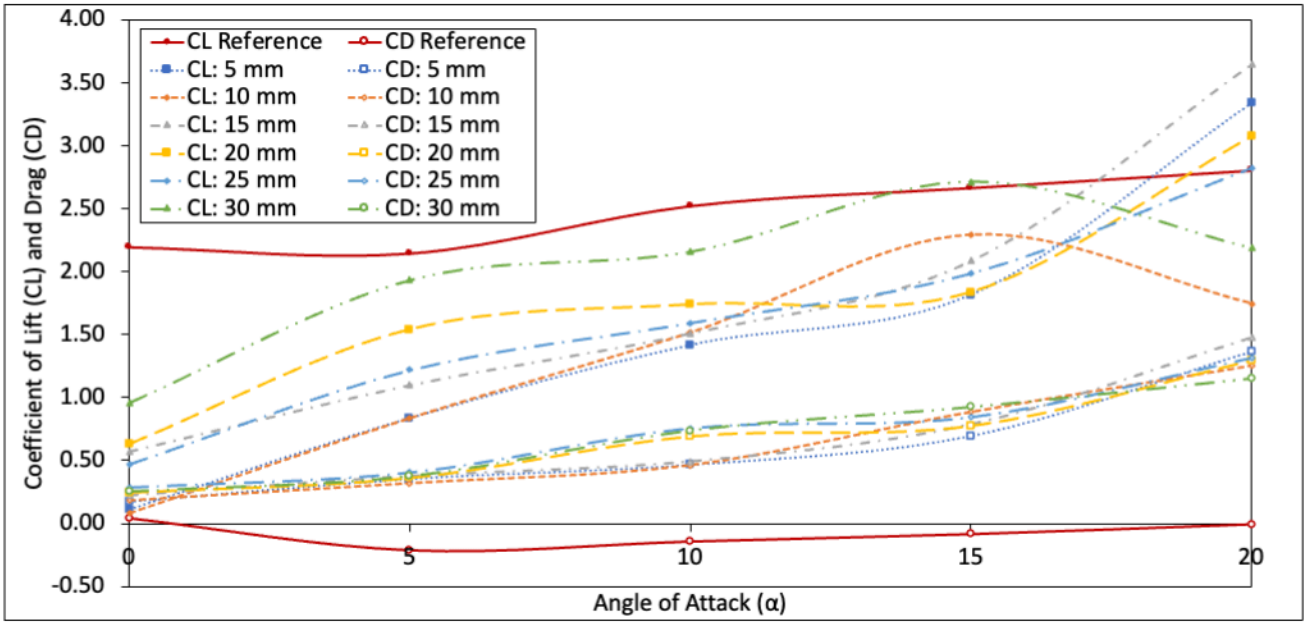

Fig. 5. Aerodynamic coefficient of CyFlaP versus α at 5 m/s inlet wind speed

The C_L in Figure 5 denotes an increment along with an increase in α yet value 56% below the reference from Ali *et al.*, [1] at $0°$. However, the closest resulting data from the reference was a 30 mm gap with a percentage difference reduced from $5°$ onwards at 10% maximum error from the reference. This matter denoted that the top plate's application was insufficient for lift generation at low inlet wind speed. Next, the C_L value plateaued for the gap of 20 mm and 30 mm from 5° to 15° of α. Hence, this factor may be affected by the swirling or losses of airspeed happening in the gap due to the low concentration flow from the entry. Therefore, a momentum injection would help to increase the air intake, thus ensuring steady air availability in the gap, based on Liang *et al.,* [21].

Next, C_{Lmax} was achieved with the highest coefficient at 15° for a 30 mm gap condition at 2% better C_L than the reference. Then, a stall occurred for the 10 mm and 30 mm gap from 15° to 20°, respectively. Concurrently, this resulted in a separation bubble atop the top plate, which worsened the aerodynamic flow of the model at stake. Despite having a lower value than the reference, the CyFlaP still encompasses attaining its lift generation without much flow disruption. A high rotational speed with higher inlet wind speed would further reduce the drag. Other than that, the overall C_D showed a high value in drag of up to 20°, which supported the theory that the attributed turbulent flow causes a decrement in the lift with an increment in drag compared to the reference. The matter was denoted by Basu [22] and Hakim *et al.*, [23] as an adverse pressure gradient that occurred when the aft ward static pressure increased with the direction of the flow. Therefore, the flow may act reversed because of the fluid particle's inadequacy in moving against the pressure gradient. Nevertheless, with reference aside, the other gap sizes showed superb aerodynamic effects where the model could attain its aerodynamic coefficients at all conditions.

With the succeeding increment in inlet wind speed, at 10 m/s, the C_L trend showed significantly better coefficients for $0°$ with a 30 mm gap at just 19% below the reference, refer to Figure 6. At high α, the trend showed an ascending coefficient beyond the reference starting from $5°$ onwards for a 30 mm gap at 7% better C_L, whereas a C_{Lmax} 31% was delineated $15°$ before entering the plateau. By looking at the trends, a gap of 10 mm and 20 mm resulted in a partial stall which can be seen from $10°$ to $15°$ but arose from $15°$ onwards. The partial stall has resulted in approximately a 2% reduction in lift, yet an increase of up to 61% and 41% better C_L than the reference and the one with a 30 mm

gap. Based on Hamisu *et al.*, [24] the occurrence of partial stall at a high gap value may be due to the portion of the model encountered stall.

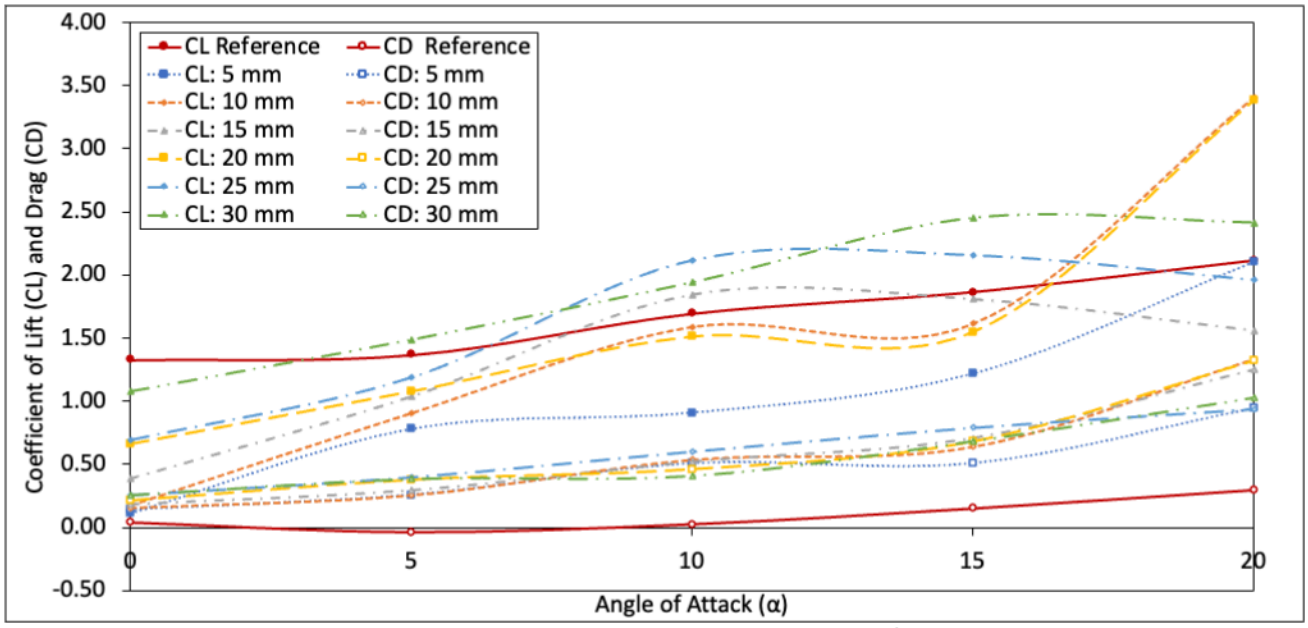

Fig. 6. Aerodynamic coefficient of CyFlaP versus α at 10 m/s inlet wind speed

After a partial stall, the part that drops will remain in that manner while the one rising will regain to produce lift, which results in its rotation. The regained manner is what has occurred at higher α. This explained that the coefficient was the best at higher α with a smaller gap application of 10 mm and 20 mm. Nonetheless, the one with a 5 mm gap had a slight plateau from $5°$ to $10°$ but then increased up to $20°$ together with the other two, 10mm and 20 mm gap. Regardless of having better C_L than the 5 m/s conditions, a reduction C_D was noted with a 45% reduction for a 15 mm gap application. Therefore, the ups and downs of the trend line were majorly affected by the placement of the top plate atop the CyFlaP, together with the inlet wind speed induced upfront.

Next, the coefficient trend showed better C_L above the reference line at higher inlet wind speed, i.e. 15 m/s, as shown in Figure 7. Here, the 30 mm gap application showed a significantly higher C_L at 24% improvement above the reference for $0°$ condition. Following this, the trends showed satisfactory results at higher α up till $15°$ with the highest C_{Lmax} at 73% above reference for 30 mm gap application before entering stall from $15°$ to $20°$ α. A partial stall can be denoted for 20 mm and 25 mm gap from $10°$ to $15°$ falls below the reference yet increased exponentially from $15°$ to $20°$ with the highest achieved by 20 mm gap at 120% better than the reference data itself.

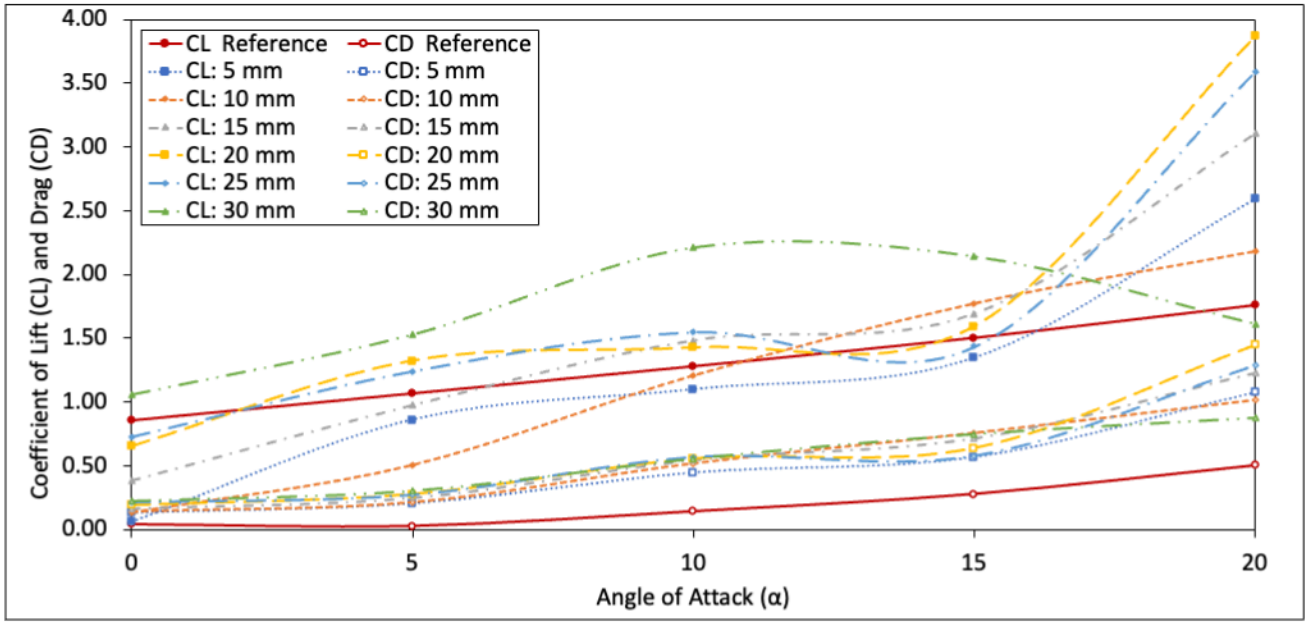

Fig. 7. Aerodynamic coefficient of CyFlaP versus α at 15 m/s inlet wind speed

Referring to the trends, gap configurations other than 30 mm demonstrated significant aerodynamic improvements, ranging from 10 mm at 24% C_L above reference to the highest improvement of 120%. The results confirm that smaller gap applications at high inlet wind speeds optimize airflow concentration, reducing flow separation effects. This configuration improves lift performance by maintaining a steady boundary layer, minimising adverse pressure gradients. However, the increase in C_L was accompanied by a rise in C_D though the percentage difference was lower than that observed at 5 m/s and 10 m/s inlet wind speeds. This indicates that while lift is enhanced, drag also increases at higher speeds due to stronger flow interactions. To mitigate this, refining the leading edge of the top plate such as implementing a smoother or rounded profile could help reduce drag and improve overall aerodynamic efficiency.

3.2 Effect on Velocity and Pressure Contours

The CFD post-processing results in Figure 8 and Figure 9 illustrate the velocity and pressure contours for the CyFlaP Magnus UAV with top plate gaps of 15 mm and 30 mm at an inlet wind speed of 15 m/s. These gap sizes were selected based on their aerodynamic performance at different angles of attack, particularly considering the key role of $0°$ in CyFlaP's flight characteristics since the CyFlaP relies on the Magnus effect for lift rather than wing incidence. Previous findings from Figure 7 showed that a 30 mm gap surpassed the reference C_L at $0°$, suggesting that increasing the gap could further influence airflow circulation and pressure distribution. The 15 mm gap represents a moderate configuration, maintaining concentrated airflow while reducing separation effects. In contrast, the 30 mm gap was chosen to examine the impact of a wider spacing on circulation and wake turbulence. These visualisations provide crucial insight into the aerodynamic behaviour, particularly in explaining why the 30 mm gap deviates from the expected trend at $0°$ and how airflow concentration affects both lift and drag performance.

For the 15 mm gap, velocity contours indicate a highly concentrated airflow between the top plate and rotating cylinders, intensifying the Magnus effect. This configuration reduces separation bubbles, stabilizes boundary layer attachment and increases lift generation, particularly at moderate angles of attack. However, the confinement of flow in a narrow gap can also lead to increased

localised pressure gradients, which may contribute to higher pressure drag. The pressure contour confirms that while lift is generated efficiently, abrupt transitions in pressure regions could be a source of additional drag.

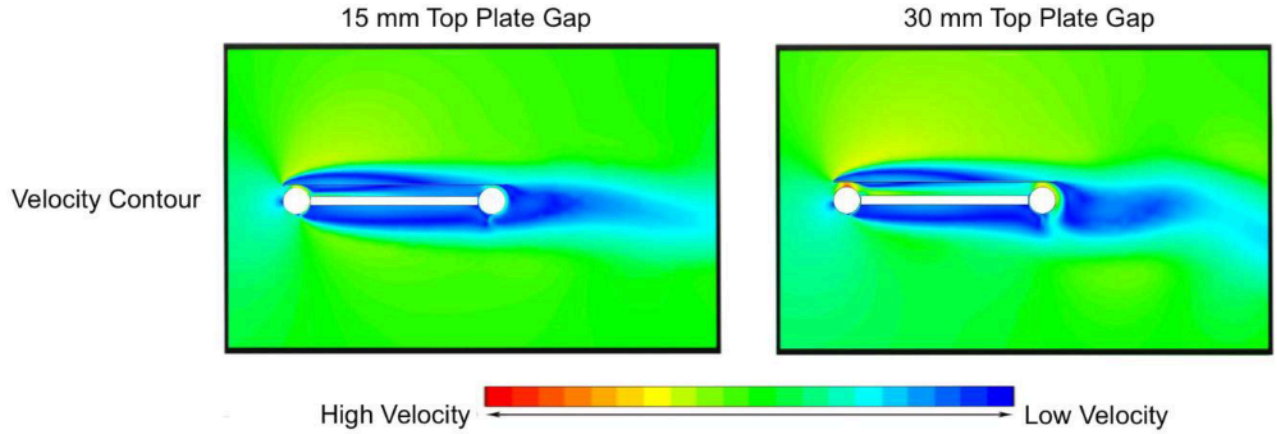

Fig. 8. Velocity contour for concentrated flow of 15 mm and 30 mm top plate gap

In contrast, the 30 mm gap exhibits a broader, more dispersed velocity distribution, initially suggesting a weaker aerodynamic advantage. However, at 0°, this wider spacing allows for enhanced circulation around the rotating cylinders, generating a more substantial low-pressure zone and a more developed Magnus effect. This explains why, despite the trend favouring smaller gaps, the 30 mm gap still surpasses the reference in lift performance at low angles.

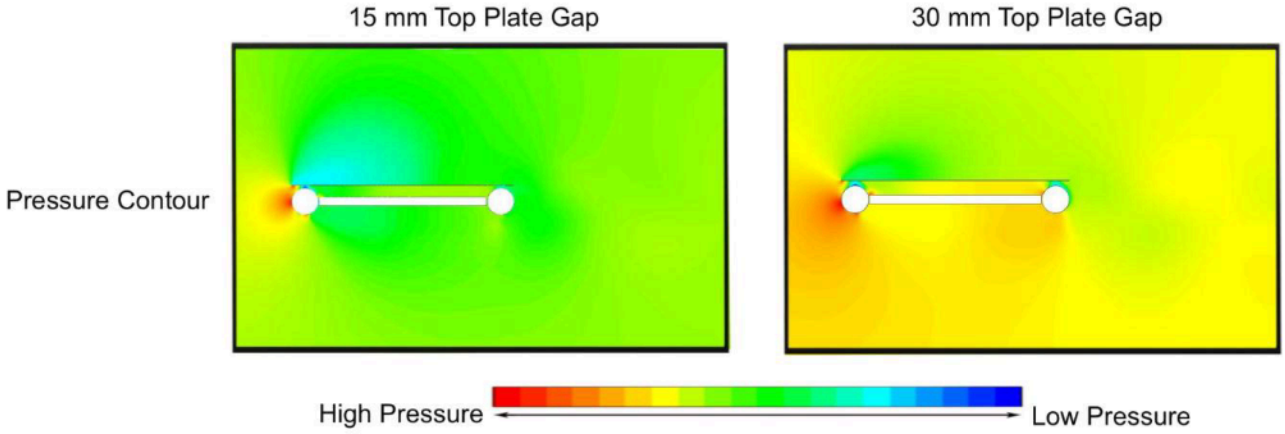

Fig. 9. Pressure contour for the concentrated flow of 15 mm and 30 mm top plate gap

The pressure contours further illustrate the interplay between airflow concentration and aerodynamic efficiency. While the 15 mm gap ensures a controlled low-pressure region, the sudden transition in flow paths could contribute to form drag. The 30 mm gap, on the other hand, shows a smoother distribution of pressure, indicating that while it benefits from increased circulation, its wake turbulence leads to higher overall drag penalties. This trade-off suggests that further refinement of the top plate's leading-edge design could mitigate drag while maintaining optimal airflow concentration. Smoothing or rounding the top plate's leading edge can reduce abrupt pressure changes, lower drag while improving boundary layer control. A more streamlined design would also enhance concentrated airflow, minimising wake turbulence and optimising aerodynamic performance.

The CFD analysis highlights how increasing velocity influences drag behaviour, driven by changes in flow separation dynamics. C_L and C_D trends indicate that smaller gaps strengthen low-pressure zones, enhancing lift at moderate angles of attack and influencing drag characteristics. At higher velocities, smaller gaps experience stronger adverse pressure gradients and wake turbulence, affecting aerodynamic performance. At higher angles of attack, smaller gaps exhibit increased drag due to intensified pressure gradients and wake turbulence, particularly at lower Reynolds numbers. As velocity decreases, flow separation exacerbates, increasing aerodynamic penalties.

In contrast, wider gaps exhibit a more gradual drag increase, benefiting from improved pressure recovery and reduced susceptibility to flow separation at higher speeds. Larger gaps show improved pressure recovery and reduced sensitivity to flow detachment, contributing to a more controlled drag response at elevated speeds. As shown in Figure 10, the velocity contours for the 30 mm gap at 20° reveal a pronounced wake region behind the CyFlaP, indicating significant flow separation. This detachment weakens the effective circulation around the rotating cylinders, disrupting the low-pressure zone that is essential for lift generation. Figure 11 further supports this observation, where the pressure contours highlight an extensive low-pressure region forming at the rear. This expanded wake region contributes to increased form drag, which counteracts lift enhancement and explains the observed drop in C_L at 20° in Figure 7. This trend suggests that while a larger gap improves circulation at lower angles of attack, it becomes less effective at higher angles due to intensified wake turbulence and reduced pressure recovery.

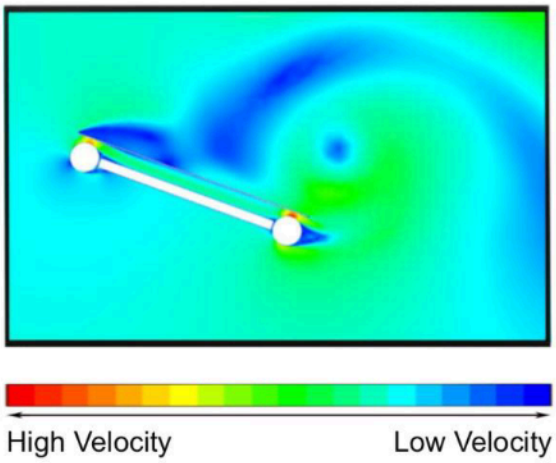

Fig. 10. Velocity contour at 20° and 15 m/s for a 30 mm gap, showing wake turbulence and flow separation

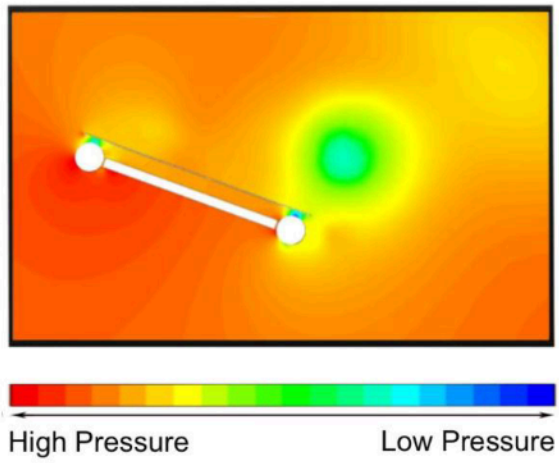

Fig. 11. Pressure contour at 20° and 15 m/s for a 30 mm gap, highlighting low-pressure wake and pressure gradients

Furthermore, the velocity contours suggest that while smaller gap configurations maintain boundary layer attachment at lower speeds, they experience earlier flow separation at higher Reynolds numbers, contributing to increased drag penalties. Conversely, larger gaps such as the 20 mm and 30 mm configurations exhibit lower drag at higher speeds due to more gradual pressure transitions but at the expense of reduced lift enhancement. This trade-off highlights the importance of optimising the gap width based on operating conditions to balance lift generation and drag minimisation.

These findings underscore the significance of aerodynamic profiling and gap parameterisation in optimising flow characteristics. While Figures 8 and 9 illustrate the velocity and pressure distributions for the 15 mm and 30 mm gaps, the aerodynamic performance trends corresponding to different gap configurations can be interpreted through the C_L and C_D data presented in Figure 5, Figure 6 and

Figure 7, respectively. These figures provide a broader perspective on the performance variations across all tested gaps, demonstrating the impact of changing flow characteristics on aerodynamic efficiency. While smaller gaps concentrate airflow for improved lift at higher angle of attack and larger gaps enhance circulation at 0°, strategic refinements in top plate geometry such as rounded leading edges could further enhance the CyFlaP's aerodynamic performance. These improvements could maximise the efficiency of Magnus-based UAV designs by addressing lift generation and drag reduction. The following section discusses the practical implications of these findings, including potential limitations and real-world implementation considerations.

3.3 Limitation and Practical Consideration

While the CFD analysis provides valuable insights into the aerodynamic performance of the modified CyFlaP Magnus UAV, certain limitations and real-world considerations must be acknowledged for practical implementation.

3.3.1 Environment variability and structural factors

The CFD simulations in this study were conducted under controlled conditions, assuming uniform airflow and steady operational parameters. However, real-world UAV applications experience variable wind conditions, turbulence and dynamic flight manoeuvres that may influence aerodynamic performance. While beneficial in concentrating airflow, the top plate design may also introduce additional structural loads that could affect UAV stability. Further studies should evaluate material selection and weight distribution to ensure the design remains aerodynamically and structurally feasible for practical deployment.

3.3.2 CFD assumptions and limitations

The study employs transient CFD simulations, allowing for analysis of unsteady flow effects, vortex shedding and time-dependent aerodynamic behaviour. While this approach captures key dynamic interactions, certain real-world complexities, such as atmospheric turbulence, UAV motion-induced effects and variable environmental conditions, are still simplified in the computational model. The cylinders' rotational speed and the top plate's gap size were also analysed under fixed conditions. Adaptive gap adjustments or variable rotation rates could further optimise performance by allowing real-time aerodynamic adjustments based on flight conditions.

Furthermore, the findings are based on specific computational conditions and their applicability in broader operational scenarios requires further validation. Future research should examine a wider range of environmental factors, including variations in air density, turbulence intensity and wind shear effects, to ensure the robustness of these aerodynamic improvements. Implementing fluid-structure interaction (FSI) analyses could also offer deeper insight into how structural deformations impact aerodynamic efficiency, particularly under fluctuating wing loads.

3.3.3 Need for experimental validation

Although transient CFD provides detailed aerodynamics insights, physical testing is necessary to confirm the computational predictions. Wind tunnel testing would allow for direct measurement of lift, drag and flow behaviour, ensuring that the top plate's influence on airflow separation is consistent under real-world conditions. Flow visualisation techniques, such as particle image

velocimetry (PIV), could also help validate how concentrated airflow influences aerodynamic efficiency.

3.4 Additional Design Recommendations

While the study demonstrates that a fixed top plate improves aerodynamic performance by concentrating airflow, further refinements could enhance lift while minimising drag. One potential improvement is modifying the leading edge of the top plate. A smoother, rounded edge could reduce abrupt pressure changes, promote better flow attachment, minimise turbulence and lower drag without compromising lift.

Another approach is the implementation of a porous or slotted top plate, allowing partial airflow to pass through. This could regulate flow separation and reduce the formation of separation bubbles, potentially enhancing aerodynamic stability. However, optimising the porosity level would be crucial to ensure airflow control without diminishing the Magnus effect.

An adjustable gap mechanism could also provide dynamic airflow control, adapting the gap size based on changing light conditions. This flexibility could optimise lift-to-drag ratios at varying speeds and angles of attack, improving overall aerodynamic efficiency. While this would introduce additional mechanical complexity, it may offer significant advantages in manoeuvrability and efficiency.

Though beyond the scope of the current computational study, these design enhancements provide a strong foundation for future investigations. Further computational testing and experimental validation could explore their feasibility and effectiveness, ensure improved performance while maintain structural efficiency.

4. Conclusions

The analysis of the modified CyFlaP with a top plate for concentrated flow demonstrates enhanced aerodynamic performance at high inlet wind speeds. Notably, the modified model achieves a 120% increase in C_L compared to the reference, confirming its enhanced lift generation. Additionally, the smaller gap configuration delays stall at high wind speeds and angle of attack, further improving stability. While the higher C_D remains a factor, smoothing the leading edge, similar to an aerofoil, could reduce drag penalties and optimise flow concentration. Further research could explore refining gap configurations to balance lift enhancement and drag reduction. Given these advancements, the modified CyFlaP presents promising applications in aerospace and Magnus UAV innovation. Additionally, experimental validations through wind tunnel testing would be crucial in corroborating the CFD findings and refining the model for real-world applications.

Acknowledgement

This research is supported by the Ministry of Education (MoE) Malaysia under the research grant scheme of Fundamental (FRGS) Phase 1/2018 with MoE ref. code FRGS/1/2018/TK09/ UPM/02/2.

References

[1] Ali, Hidayatullah Mohammad, Azmin Shakrine Mohd Rafie, Syaril Azrad Md Ali and Ezanee Gires. "Computational analysis of the rotating cylinder embedment onto flat plate." *CFD Letters* 13, no. 12 (2021): 133-149. https://doi.org/10.37934/cfdl.13.12.133149

[2] Ali, Hidayatullah Mohammad, Azmin Shakrine Mohd Rafie and Syaril Azrad Md Ali. "Numerical analysis of leading edge cylinder Aerofoil on Selig S1223 for moving surface boundary control." *Journal of Aeronautics, Astronautics and Aviation* 53, no. 2 (2021): 143-153.

[3] Modi, V. J. "Moving surface boundary-layer control: a review." *Journal of fluids and structures* 11, no. 6 (1997): 627-663. https://doi.org/10.1006/jfls.1997.0098
[4] Modi, V. J., M. S. U. K. Fernando and T. Yokomizo. "Moving surface boundary-layer control-Studies with bluff bodies and application." *AIAA journal* 29, no. 9 (1991): 1400-1406. https://doi.org/10.2514/3.10753
[5] Guo, Xiao-hui, Jian-zhong Lin, Cheng-xu Tu and Hao-li Wang. "Flow past two rotating circular cylinders in a side-by-side arrangement." *Journal of Hydrodynamics* 21, no. 2 (2009): 143-151. https://doi.org/10.1016/S1001-6058(08)60131-6
[6] Alias, M. S., AS Mohd Rafie, O. F. Marzuki, MF Abdul Hamid and C. C. Chia. "Two dimensional numerical analysis of aerodynamic characteristics for rotating cylinder on concentrated air flow." In *IOP Conference Series: Materials Science and Engineering*, vol. 270, no. 1, p. 012003. IOP Publishing, 2017. https://doi.org/10.1088/1757-899X/270/1/012003
[7] Ali, Hidayatullah Mohammad, Azmin Shakrine Mohd Rafie, M. F. A. Hamid and S. A. M. Ali. "Comparative Computational Study of Double Rotating Cylinder Embedded on Selig S1223 Aerofoil and Flat Plate for High Altitude Platform." *Pertanika J. Sci. Tech* 30 (2022): 2767-2788. https://doi.org/10.47836/pjst.30.4.26
[8] Arif, Nur Liyana Sabrina Muhd, Hidayatullah Mohammad Ali and Azmin Shakrine Mohd Rafie. "Computational Aerodynamics Analysis On Pitching Moment Using Ducted Fan Over Flat Plate For High Altitude Platform Station." *Journal of Aerospace Society Malaysia* 1, no. 1 (2023): 23-33.
[9] Kamid, Muhammad Irfan, Hidayatullah Mohammad Ali and Azmin Shakrine Mohd Rafie. "Computational Aerodynamics Analysis Of A Bluff Body With Rotating Cylinder As Drag Reducer." *Journal of Aerospace Society Malaysia* 1, no. 1 (2023): 34-45.
[10] Roslan, Muhammad Syakir Iman, Hidayatullah Mohammad Ali and Azmin Shakrine Mohd Rafie. "Rotational Speed Analysis on Double Rotating Cylinder for Cylinder to Flat Plate using Numerical Method." *Journal of Aeronautics, Astronautics and Aviation* 55, no. 3S (2023): 495-506.
[11] Zaimi, Ummi Zuhairah, Hidayatullah Mohammad Ali and Azmin Shakrine Mohd Rafie. "Experimental Analysis on Pitching Moment for Embedment Cylinder to Flat Plate High Altitude Platform Station." In *International Seminar on Aeronautics and Energy*, pp. 197-209. Singapore: Springer Nature Singapore, 2022. https://doi.org/10.1007/978-981-99-6874-9_16
[12] Subramaniam, Kamalleswaran and Wan Saiful-Islam Wan Salim. "A Review of Experimental Approaches for Investigating the Aerodynamic Performance of Drones and Multicopters." *Journal of Advanced Research in Experimental Fluid Mechanics and Heat Transfer* 14, no. 1 (2023): 1-24. https://doi.org/10.37934/arefmht.14.1.124
[13] Wang, Shizhao, Xing Zhang, Guowei He and Tianshu Liu. "A lift formula applied to low-Reynolds-number unsteady flows." *Physics of Fluids* 25, no. 9 (2013). https://doi.org/10.1063/1.4821520
[14] Badalamenti, Carmine and Simon Prince. "Effects of endplates on a rotating cylinder in crossflow." In *26th AIAA Applied Aerodynamics Conference*, p. 7063. 2008. https://doi.org/10.2514/6.2008-7063
[15] Barati, Ebrahim, Mehdi Rafati Zarkak and Javad Abolfazli Esfahani. "Effect of rotational direction of circular cylinder for mixed convection at subcritical Reynolds Number." In *27th Annual International Conference of Iranian Society of Mechanical Engineers (ISME 2019)*, pp. 1-6. 2019.
[16] Torres, Gabriel Eduardo. *Aerodynamics of low aspect ratio wings at low Reynolds numbers with applications to micro air vehicle design*. University of Notre Dame, 2002.
[17] Abdulla, Najdat Nashat and Mustafa Falih Hasan. "Effect of gap between airfoil and embedded rotating cylinder on the airfoil aerodynamic performance." *Research & Development in Material Science* 3, no. 4 (2018): 1-10. https://doi.org/10.31031/RDMS.2018.03.000567
[18] Mgaidi, A. M., A. S. Rafie, K. A. Ahmad, R. Zahari, MF Abdul Hamid and O. F. Marzuki. "Numerical and experimental analyses of the flow around a rotating circular cylinder at subcritical regime of reynolds number using k-ε and k-ω-sst turbulent models." *ARPN Journal of Engineering and Applied Sciences* 13, no. 3 (2018): 954-960.
[19] Menter, Florian R. "Two-equation eddy-viscosity turbulence models for engineering applications." *AIAA journal* 32, no. 8 (1994): 1598-1605. https://doi.org/10.2514/3.12149
[20] Yao, Q., C. Y. Zhou and C. Wang. "Numerical study of the flow past a rotating cylinder at supercritical Reynolds number." In *2016 4th International Conference on Mechanical Materials and Manufacturing Engineering*, pp. 667-670. Atlantis Press, 2016. https://doi.org/10.2991/mmme-16.2016.159
[21] Liang, Chua Bing, Akmal Nizam Mohammed, Azwan Sapit, Mohd Azahari Razali, Mohd Faisal Hushim, Amir Khalid and Nurul Farhana Mohd Yusof. "Numerical simulation of aerofoil with flow injection at the upper surface." (2021).
[22] Basu, P. "Boundary layer with pressure gradient." *Greenfield Research Inc., 18. Greenfield Research Inc* (2001).
[23] Hakim, Muhammad Syahmi Abdul, Mastura Ab Wahid, Norazila Othman, Shabudin Mat, Shuhaimi Mansor, Md Nizam Dahalan and Wan Khairuddin Wan Ali. "The effects of Reynolds number on flow separation of Naca Aerofoil." *Journal of Advanced Research in Fluid Mechanics and Thermal Sciences* 47, no. 1 (2018): 56-68.

[24] Hamisu, Muhammad Tukur, Mahmud Muhammad Jamil, Umar Sanusi Umar and Aisha Sa'ad. "Numerical study of flow in asymmetric 2D plane diffusers with different inlet channel lengths." *CFD Letters* 11, no. 5 (2019): 1-21.